Journal of
Manufacturing and Materials Processing

MDPI

Article

Semi-Continuous Functionally Graded Material Austenitic to Super Duplex Stainless Steel Obtained by Laser-Based Directed Energy Deposition

Juan Carlos Pereira *, David Aguilar, Iosu Tellería, Raul Gómez and María San Sebastian

LORTEK Technological Centre, Basque Research and Technology Alliance BRTA, Arranomendia Kalea 4A, 20240 Ordizia, Gipuzkoa, Spain; daguilar@lortek.es (D.A.); itelleria@lortek.es (I.T.); rgomez@lortek.es (R.G.); msansebastian@lortek.es (M.S.S.)
* Correspondence: jcpereira@lortek.es; Tel.: +34-943-882-303

Abstract: In this work, a semi-continuous functionally graded material (FGM) between an austenitic and a super duplex stainless steel was obtained. These materials are of great interest for the chemical, offshore, and oil and gas sectors since the austenitic stainless steel type 316L is common (and not so expensive) and super duplex stainless steels have better mechanical and corrosion resistance but are more expensive and complex in their microstructural phases formation and the obtention of the balance between their main phases. Using directed energy deposition, it was possible to efficiently combine two powders of different chemical compositions by automated mixing prior to their delivery into the nozzle, coaxially to the laser beam for melting. A dense material via additive manufacturing was obtained, with minimum defectology and with a semi-continuous and controlled chemical compositional gradient in the manufactured part. The evolution of ferrite formation has been verified and the phase fraction measured. The resulting microstructure, austenite/ferrite ratio, and hardness variations were evaluated, starting from 100% austenitic stainless-steel composition and with variants of 5% in wt.% until achieving 100% of super duplex steel at the end of the part. Finally, the correlation between the increase in hardness of the FGM with the increase in the ferrite phase area fraction was verified.

Keywords: functionally graded material; metal additive manufacturing; directed energy deposition; laser metal deposition; austenitic stainless steel; super duplex stainless steel

Citation: Pereira, J.C.; Aguilar, D.; Tellería, I.; Gómez, R.; San Sebastian, M. Semi-Continuous Functionally Graded Material Austenitic to Super Duplex Stainless Steel Obtained by Laser-Based Directed Energy Deposition. *J. Manuf. Mater. Process.* **2023**, *7*, 150. https://doi.org/10.3390/jmmp7040150

Academic Editors: Mohsen K. Keshavarz, Esmaeil Sadeghi and Steven Y. Liang

Received: 28 June 2023
Revised: 6 August 2023
Accepted: 10 August 2023
Published: 12 August 2023

1. Introduction

Obtaining functionally graded materials (FGMs) has been challenging so far; one of the pioneers was Soodi et al. [1]. However, with the emergence and industrialization of metal additive manufacturing (AM) processes such as directed energy deposition (DED) technologies, it is possible to fabricate complex parts with functional gradients [2]. A major advantage of DED technology is its ability to produce multi-material components with key importance in solving long-standing problems in dissimilar metal welding and alloy development. Some examples of multi-material DED parts are rocket nozzle prototypes (Nimonic75 + IN718 in outer and Al-bronze for cooling channel and inner sections) [3,4] and slide bearings for shafts (steel and bronze in one part) [5]. Since some laser-based DED processes rely on the use of blown powder as raw material (DED-LB/p, also known as laser metal deposition, LMD), the ability to mix various powders (in a controlled manner) in situ (i.e., during powder feeding and/or delivery) easily enables the production of complex functional gradients, multi-material layers, and even composites that can include many classes or types of materials [6], including the stainless-steel (SS) alloys. This opens a new horizon for alloy development and innovative industrial applications. Furthermore, in the research field on FGMs obtained by DED powder-blowing processes, the powder delivery

flow rate and its stability after the mixture of two chemical compositions is a key parameter to control the variability of these processes [7].

The automated industrial DED-LB/p process for multimaterial component manufacturing is associated with a variety of challenges. These include the material-dependent powder conveying behavior, the dynamics of the powder-conveying system, and design and manufacturing strategy integration [8]. Multiple studies and scientific publications dealing the study of FGMs obtained by DED using austenitic stainless steel [9] as a part of the combination [10,11] have been recently presented; however, the use of super duplex (SD) stainless steels in powder format as a feedstock has not been reported in FGMs obtained by DED-LB/p (aka LMD). Some studies have presented metal AM DED using wire as a feedstock and the processing of this type of material [12–15], evidencing its good processability via laser; however, it was difficult to control the as-built microstructure [14], oxide inclusions [16], and austenite/ferrite phase balance [17]. The four most-studied duplex alloy types in DED are (i) the so-called "lean duplex" steel type UNS S32101 (DIN 1.4162) [17], (ii) the standard duplex steel type UNS S32205 (DIN 1.4462 / Sandvik SAF2205) [12,14,15,17–19], (iii) the duplex stainless steel type 2209 in wire format (EN ISO 14343-A) [12,14,15] and (iv) recently, a third super duplex steel type UNS S32750 (DIN 1.4410/Sandvik SAF2507) [13,17,20] has also received considerable attention as a potential material for a wide range of applications in the oil and gas and refining sectors [21]. The combination of austenitic and duplex stainless steels is of high interest in the case of valves, meters, and other equipment used in the oil and gas industry. In the critical review work conducted recently by Feenstra et al. [22], the combination of SS 316L and SAF 2507 alloys was not reported for bimetallic structures and functionally graded materials produced via directed energy deposition techniques.

With the development of new FGMs, it will be possible to optimize the use of expensive or strategic materials for Europe in different areas of the part which have more demanding requirements. There is a lack of knowledge on how the microstructure and solidification modes evolve with the semi-continuous variation in the proportions of the compositions that make up the powder mixture and their fusion during the direct laser metal deposition process for the additive manufacturing of FGMs, and how it impacts the mechanical properties and performance of the new material.

Advanced multi-material manufacturing reduces the complexity of assembly, increases functionality, and reduces the costs of optimizing the part geometry and the sizes of components produced with conventional manufacturing processes in single materials. The purpose of this research work was to obtain an FGM via the combination of austenitic stainless steel and super duplex stainless steel in the same component in order to discern the minimum semi-continuous gradient that can be generated. After phase fraction and hardness measurements and the microscopy analysis were conducted, it was possible to evaluate how the microstructure, balance of austenite/ferrite, and hardness evolve in the functionally graded material obtained by the metal AM process.

2. Materials and Methods

This section summarizes all feedstock materials, microstructural characterization procedures, hardness testing equipment, laser material processing equipment, and methods that were used in this work.

2.1. Materials Characterization—Equipment and Methods

The macro and microstructural analysis was carried out using light optical microscopy (LOM) at different magnifications (from 100× to 1000×) with an Olympus GX51 optical microscope with an image acquisition system via digital camera. The chemical etching was carried out via different methods: electrolytic etching with KOH or oxalic solution and manual etching with Beraha's reagent (20 mL HCl + 100 mL H_2O + 1g $K_2S_2O_5$) for 12 s. The best results for phase identification were achieved with the use of different reagents and considering the chemical composition of the material in different zones of the FGM, similar

to that reported by Fedorov, et al. [23]. For more advanced studies in the microstructure, a field emission scanning electron microscope (FESEM) Zeiss Ultra Plus model equipped with an X-ray detector from Oxford instruments (X-Max) was also used.

The area fraction of the main phases (in percentage) was quantified by making measurements via image analysis from the micrographs. In this case, 5 LOM images were taken at 200× magnification of different areas of the central part of the layers manufactured with each powder mixture ratio, and then the images were binarized to contrast each phase, and the area represented by each phase was thereafter measured to calculate the percentage it represented. Microhardness Vickers measurements were taken in an EmcoTest DuraScan durometer using a load of 100 g (HV0.1 scale).

2.2. Feedstock Powders Characterization

In this work, two commercial gas-atomized powders were used. One was the austenitic stainless steel type 316L (AISI 316L or UNS S31603) manufactured by Flame Spray Technologies B.V. and the other was super duplex stainless steel type SAF 2507 (UNS S32750) manufactured by Sandvik Osprey®. Both powders are inert and gas-atomized and commercially available with different granulometries. In the case of the super duplex stainless steel, a vacuum induction melting and inert gas atomization (VIGA) process was used. SS316L powder was obtained by a single gas-atomization process with argon as the inert gas.

Both powders were sieved to achieve a particle size of $+45 - 106$ µm and $+45 - 90$ µm for SS 316L and SAF 2507 alloys, respectively, according to the technical specifications provided by manufacturers. The plates used as substrates (10 mm thickness) were manufactured with an austenitic stainless steel type SS 310 (UNS S31000) and provided in a soft condition (hot-rolled and annealed). The chemical compositions reported by the powder manufacturers are shown in Table 1.

Table 1. Chemical composition for each powder batch of SS 316L and SAF 2507 commercial powders used in this work (data obtained from the quality certificates of each provider).

Powder	Chemical Composition (wt.%)												
	Cr	**Ni**	**Mo**	**Mn**	**Si**	**Ti**	**Al**	**C**	**P**	**S**	**N**	**Fe**	**Rest**
SS 316L	17.1	13.0	2.59	1.2	0.56	---	---	0.03	0.010	0.010	0.06	65.37	0.04
SAF 2507	24.8	7.1	3.92	0.8	0.50	0.009	0.015	0.02	0.008	0.006	0.30	62.42	0.10

As a feedstock material quality check procedure, the powder particle batches were characterized and analyzed using LOM and FESEM images. Both powders had adequate flowability and particle size distribution for the LMD process with a coaxial nozzle. The particles' morphology is shown in the FESEM micrographs of Figure 1a,b, and the calculated particle size distributions (PSD curves) are shown in Figure 1c,d. It was confirmed that the SS 316L powder particles had a particle size distribution with a higher quantity of large particles but of a smaller average size than those of the SAF 2507 powder. In any case, the particle size range of both powders was quite similar.

The austenitic stainless-steel particles have a less spherical (lower circularity) and more irregular morphology than those of super duplex and with the presence of more satellites adhered to the particles after their gas atomization process manufacturing. Super duplex powder particles are observed to be more spherical in morphology and with fewer satellites but also present some elongated particles. After measurements, the flowability, apparent density, and circularity of super duplex particles are better than austenitic stainless-steel particles, but with a higher level of internal porosity, which can be detrimental, as trapped gas can remain after solidification of the metal following the melting and DED process. The comparative measurements of both powders are compiled in Table 2.

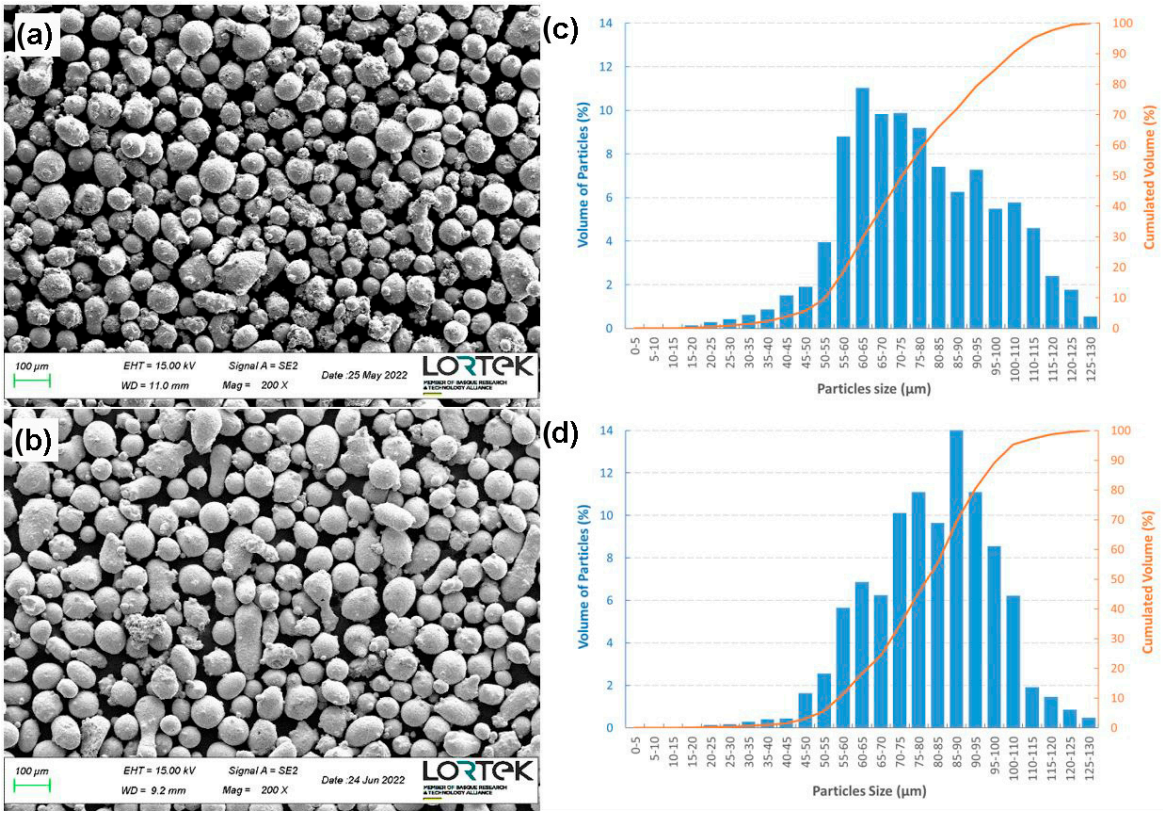

Figure 1. Micrographs of powder particles by FESEM (200× and BSE mode): (**a**) SS 316L powder and (**b**) SAF 2507 powder. Histograms of the PSD: (**c**) SS 316L powder and (**d**) SAF 2507 powder.

Table 2. Results of measurements for austenitic and super duplex stainless-steel powders.

Powders	Flowability (s/50 g @ 22 °C) (ASTM B213)	Apparent Density (g/cc^3) (ASTM B212)	Particle Size Parameters (µm)			Particles Circularity (%)	Internal Porosity (%)
			D10	D50	D90		
SS 316L	25.96 ± 0.07	4.02 ± 0.05	55.15	75.40	108.84	~46	0.27 ± 0.21
SAF 2507	17.19 ± 0.04	4.14 ± 0.05	58.80	82.24	101.55	~60	0.49 ± 0.28

2.3. Laser Metal Deposition Equipment and Set-Up

The system used for the DED-LB/p process (also known as LMD) was a four-axis Cartesian kinematic station equipped with a classical CNC table/system (FAGOR 8070, Arrasate, Spain) and a solid-state 5 kW disc laser source (Trumpf TruDisk 6002, Ditzingen, Germany) operated in continuous wave mode with a wavelength of 1030 nm. The laser beam was guided through an optic fiber of 400 µm (see Figure 2). The configuration of the LMD station includes a motorized optic head (Trumpf BEO D70, Ditzingen, Germany) with collimation/focal lengths of 100/200 mm. For powder delivery, the LMD station had a powder feeder with two 5L heated hoppers (Oerlikon Twin 150, Zürich, Switzerland) and a three-jet discrete nozzle (3-Jet-SO16-F manufactured by FhG ILT, Aachen, Germany). Argon was used as the protective gas (8 L/min) and as the carrier gas (2 L/min flow at 2 bar) for each powder delivery.

For this work, a powder mixing chamber, rapid switches for automatic hopper switching, and a powder flow watch sensor were incorporated into the twin powder-feeder system. The operating parameters were adjusted to achieve a controlled powder flow rate that adds up to a total rate of 5 g/min (SS 316L + SAF 2507 mix). The other manufacturing process parameters used were a laser spot diameter of 2.2 mm, laser power of 700 W, and deposition rate of 600 mm/min. Figure 2 shows the LMD station used, the discrete three-jet

coaxial nozzle, and the manufactured tube with a gradual chemical composition (in Z direction). The final dimensions of the manufactured single wall tube were an outside diameter of 41.2 mm, an inside diameter of 36.8 mm, and a height of 28.4 mm.

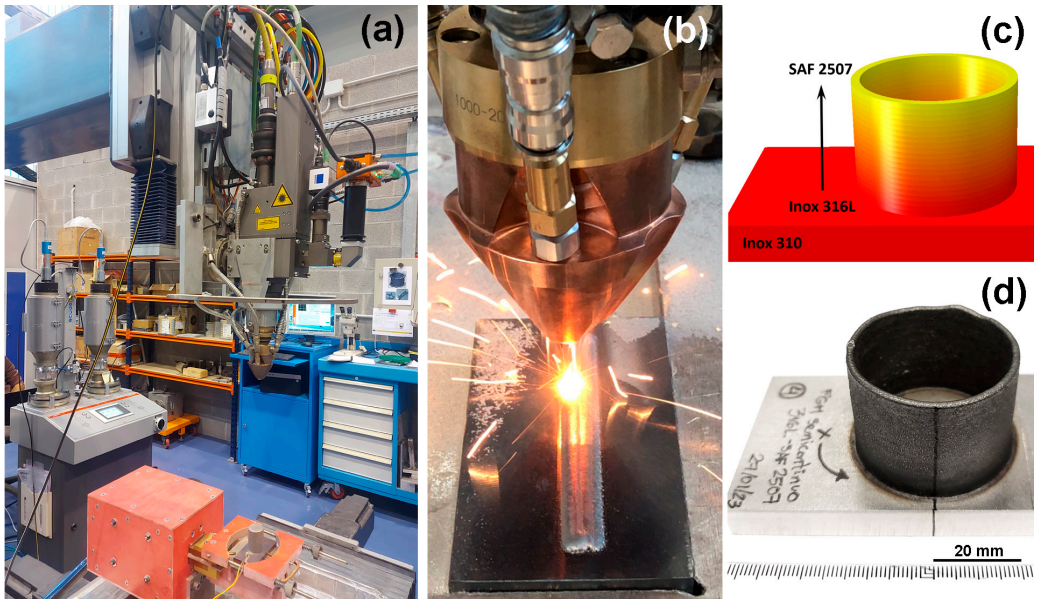

Figure 2. Details of the LMD station and FGM tube. (**a**) Cartesian four-axis kinematic LMD station at LORTEK, (**b**) details of the coaxial discrete three-jet nozzle in operation, (**c**) build direction of the semi-continuous FGM SS 316L to SAF 2507 tube, and (**d**) picture of the FGM hollow cylinder (tube) manufactured by LMD process.

The first tests were carried out by depositing a simple long track, starting with a chemical composition of 100% 316L austenitic stainless steel and gradually adding a specific amount of super duplex powder to achieve a chemical composition of 100% super duplex stainless steel by the end of the process. After the analysis of the monitored powder flow rates signals, it became evident that the total flow was not constant and was decreasing, partly due to inadequate gravimetric control of the super duplex powder, which was not increased in the necessary proportion to maintain the required total mass flow rate in g/min, among other problems.

After detecting the causes of the problems (bad connections of the super duplex powder line to the mixer and excessive length of the pipe in the lines) and after the correct integration of the mixing chamber device with better control of the rapid switch valves between hoppers and their activation sequence, plus an adequate gravimetric control, the problems were solved. For full system calibration, an individual gravimetric analysis per hopper considering the specific material density was conducted; after that, a more homogeneous and stable mixing flow was achieved for 5% increments (wt.%) in the proportion of both materials.

As a next step, and after adjusting the powder mixing system with a proper gravimetric calibration in the powder dosing of materials coming from each hopper, it was possible to manufacture a tube (single bead per layer) consisting of 63 layers with a layer height of 0.45 mm. The manufacturing started with 100% of 316L stainless-steel powder; every three layers, the mixing ratio between the austenitic SS and the super duplex SS powder flow was changed, reducing the amount of austenitic SS at 5 wt.% whilst adding 5 wt.% of the super duplex SS in the mass flow. In other words, the chemical composition of the FGM material was changed in a semi-continuous way every three layers, decreasing the amount of austenitic stainless steel and increasing the amount of super duplex, until finishing with 100% super duplex stainless steel in the last three layers.

3. Results and Discussion

3.1. LMD Process Development and Adjusting to Obtain a Semi-Continuous Graded Material

For the study of semi-continuous multi-material deposition (gradual transition or combination between two materials), the capability of the powder feeding and mixing system incorporated in the LMD cell to deposit a functional graded material was analyzed. The system was tuned and adjusted to combine a certain proportion of powder from one hopper (austenitic stainless steel type 316L) with another proportion of powder from a second hopper (super duplex steel SAF 2507) in a mixing chamber device. The difficulty here lies in achieving a stable powder mix flow rate and in achieving a certain level of automation and control in the command of the operation parameters for each hopper in the twin powder feeder and the mixing system to obtain the minimum composition gradient change and the precise proportion that is required at the time or position of the nozzle that is desired. The main objective of the study was to analyze and discern the minimum discontinuous gradient that can be achieved during the laser direct deposition process to make it possible to either fabricate with a semi-continuous gradient in the layers of a 2.5D fabrication (functional gradient in the Z direction, as shown in Figure 2c). The analysis could also be used to obtain an FGM in the same layer (functional gradient in the radial or X/Y direction from the center outwards or vice versa).

Figure 3 shows the monitored data (powder mass flows) in the manufacturing of the continuous deposition tube. The delay time on the powder delivery was mainly affected by the conveyer line length and the carrier gas flow rate [8]; for this work, the delay time was well established for the LMD process parameters defined and after multiple trials conducted before the FGM tube manufacturing.

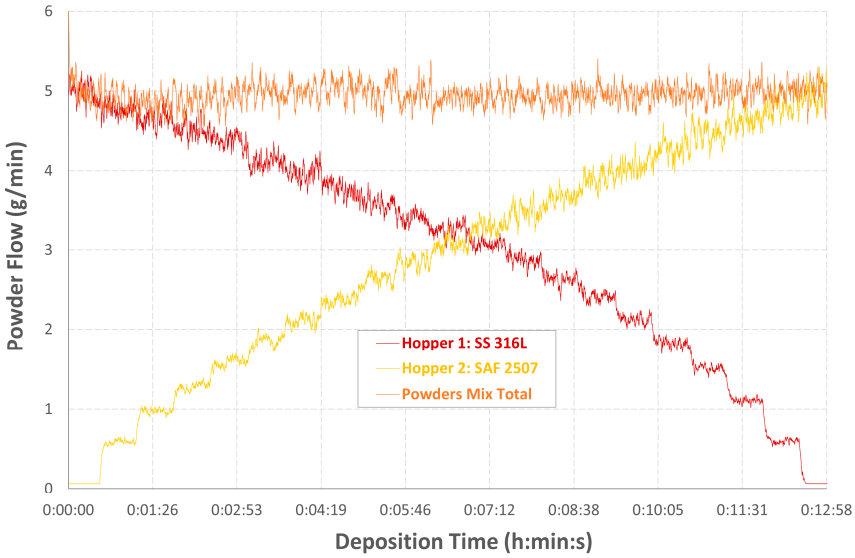

Figure 3. Example of powder flow monitoring on each hopper and at the nozzle inlet in a deposition test for a semi-continuous FGM SS 316L+SAF 2507 after gravimetric control and system tuning.

Powder mix samples were taken at the nozzle outlet with different mixing proportions, with the laser off, to observe them in a FESEM and evaluate the homogeneneity of the particle mixture of both materials. The chemical composition, being similar in the two materials of the gradient created, makes it difficult to discriminate the particles using EDS maps, which was attempted without success.

3.2. Cross-Section and Microstructure Analysis by LOM

The manufactured FGM tube was cut to evaluate its cross-section, and after metallographic preparation of the sample, the predominant microstructure in the material obtained with the combination of powders was revealed after using suitable chemical etching. In the polished state, we found minimal flaws, in the form of small and rounded internal

porosities in the deposited material, evaluated in the cross-section of the tube. This porosity seems to be gas trapped during the solidification process of the deposited graded material. After analyzing the internal porosity of the particles of each powder provider (reported in Table 2), we observed that in the coarse particles of both gas-atomized powders' internal porosities (see Figure 4), which were in a major proportion in the super duplex steel powder particles. We presumed that these particles' porosities could generate gas trapped in the melt pool that is grouped and does not escape from the molten metal due to the high deposition speed and specific solidification conditions in the single-track deposition process and that generates such a defect.

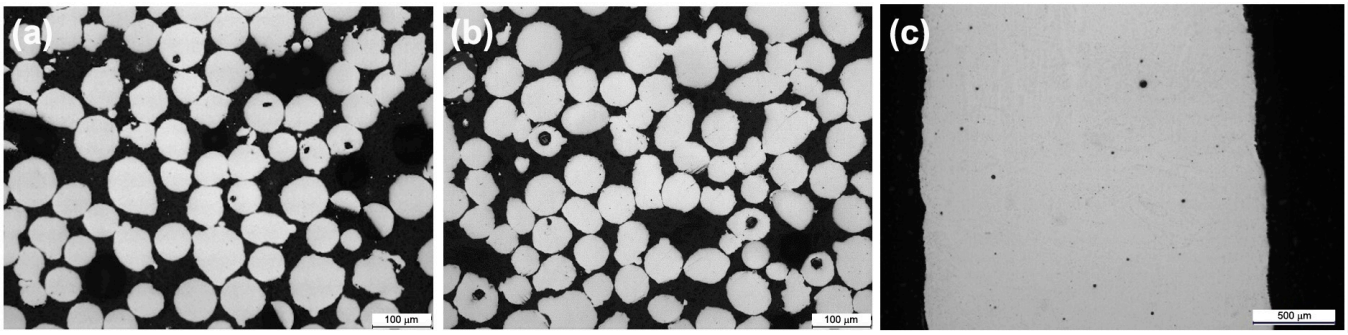

Figure 4. LOM micrographs (polished condition). (**a**) Cross-section of SS 316L powder particles, (**b**) cross-section of SAF 2507powder particles, and (**c**) cross-section of the manufactured FGM tube (details of the last three layers deposited with a composition of 100% SAF 2507).

In the etched condition and for the layers with the highest AISI 316L content, an electrolytic KOH solution was used as the reagent, and for the layers with the highest super duplex content, chemical etching by immersion with Beraha's reagent was subsequently used. In Figure 5, the optical micrographs of each combination are compiled for comparison. They show the evolution between the proportion of austenite and ferrite with the progression in the semicontinuous chemical gradient in the central area of each deposited layer. The substrate material and potential dilution effect were not considered in this study.

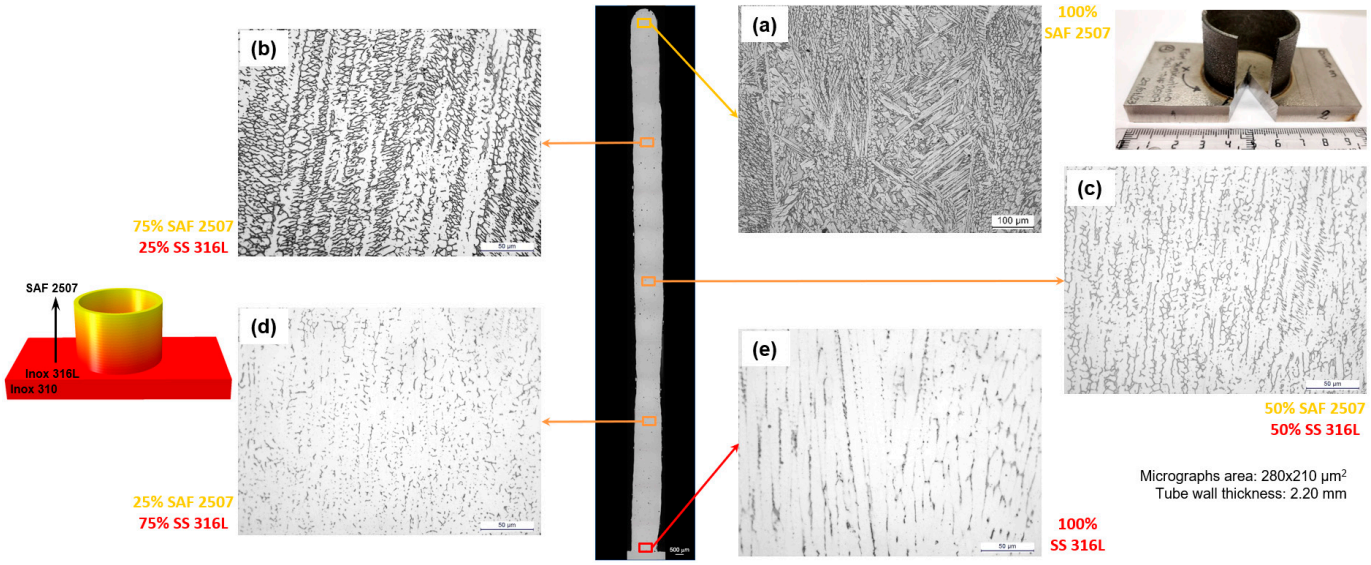

Figure 5. Cross section of the FGM tube deposited with different balances (in wt.%) of austenitic/super duplex stainless-steel compositions (LOM micrographs, at 200× and 500× electrolytic etching with KOH solution). (**a**) 100/0, (**b**) 75/25, (**c**) 50/50, (**d**) 25/75, and (**e**) 0/100.

The process by which the microstructure of the material evolves with the functional gradient of the chemical composition, not only in the columnar dendritic growth form,

but also in the size of the dendrites and formation of main phases, is clearly observed in the micrographs of Figure 5. The initial microstructure of the 316L austenitic stainless steel obtained by LMD is of the cellular dendritic type (see the micrographs with different proportions of elements in Figure 5) with an epitaxial grain nucleation mechanism and columnar dendritic growth of columnar grains in the direction of the maximum thermal gradient (towards the surface of the layers); progressing through a competitive growth mechanism, this microstructure, at least for austenitic SS 316L compositions, is similar to those reported in the literature [24]. Small cells of the delta ferrite phase (δ, in the form of needles and plates) were observed in the austenitic matrix of gamma iron austenite (γ) dendrites. Some authors report the presence of a Laves phase [25], which was not observed in the evaluated layers with LOM; a reduced fraction of the gamma-prime phase (γ') could have been present but was not observed by optical microscopy in the zones with higher SS 316L content.

The solidification mode in DED processing of austenitic stainless steels influences the partitioning of alloying elements in regions of compositional microsegregation, the morphology and volume fraction of retained ferrite, and the development of grain boundaries in as-deposited materials [26,27]. In a sequence depicting microstructural development, the first act is the oxide inclusion formation, followed by a dislocation substructure, primary ferrite (FA) cellular solidification structure (in the case of austenitic SS compositions), or primary austenite (AF) cellular solidification structure (in the case of ferritic SS compositions), creating the epitaxial grain structure [26,28]. The primary phase formed from the liquid (L) may be austenite (γ) or ferrite (α) depending on the content of austenite- and ferrite-stabilizing elements, such as Ni and Cr, respectively. For the austenitic SS composition, grain morphology and size are related to the solidification mode with primary austenite solidification (AF) due to the prevalence of the 316L composition.

With the progressing of the FGM, the residual primary ferrite results from incomplete delta to gamma transformation during solidification and/or residual ferrite after Widmanstatten austenite precipitation in primary ferrite. This proposed solidification path is based on the classical metallurgical theory of stainless steel welding and considers only the chemical composition [29,30]. The transition in the solidification modes along the build-up is as shown in Figure 5c–e. According to different authors, the intragranular austenite in the as-deposited microstructure was found to preferentially nucleate and grow from inclusions [17,31].

The duplex microstructure observed on the last three deposited layers could be influenced not only by the austenite formation from the primary ferrite (FA) mechanism, but also by the solidification conditions and thermal gradients derived from the different thermal conductivity in this material, the increased heat exchange surface, and the distance from the build plate. However, this microstructure is quite similar to that reported by other authors who have deposited super duplex SS via the DED-LB/p process [13,17,31] and the DED-LB/w process [14,15].

3.3. FESEM and EDS Analysis in the FGM Obtained

Ferrite and austenite phases in different ratios were observed in the microstructure of the FGM in as-built conditions, as indicated previously. The elongated grains of ferrite grow through several layers and there are fine-grained areas along the boundaries of the melt pool region. The austenitic phases in three variants form during deposition following a cooling and thermal cycle. Grain boundary austenite was formed first along ferrite grain boundaries at the highest temperatures between 1350 °C and 850 °C [32]; Widmanstätten austenite creates thin needles, whereas the intergranular austenite precipitates as fine particles within ferrite grains at the lowest solidification temperature and preferentially nucleate and grow from oxide inclusions. All types of austenite are visible in micrographs of upper layers in the as-built condition (see Figure 6c). Ferrite grains in the etched samples grew across several layers of the build, similar to those reported in the literature when a wire super duplex was used as the feedstock [15]. Additionally, the presence of some

oxygen-rich inclusions rich in Mn and Si were observed in the microstructure, similar to those previously reported by Smith et al. [26]. Oxide inclusions nucleate and grow when the solubility of oxygen dissolved in the molten pool decreases, these inclusions were identified as metastable rhodonite ($MnSiO_3$ or $MnO.SiO_2$) by Iams et al. [31].

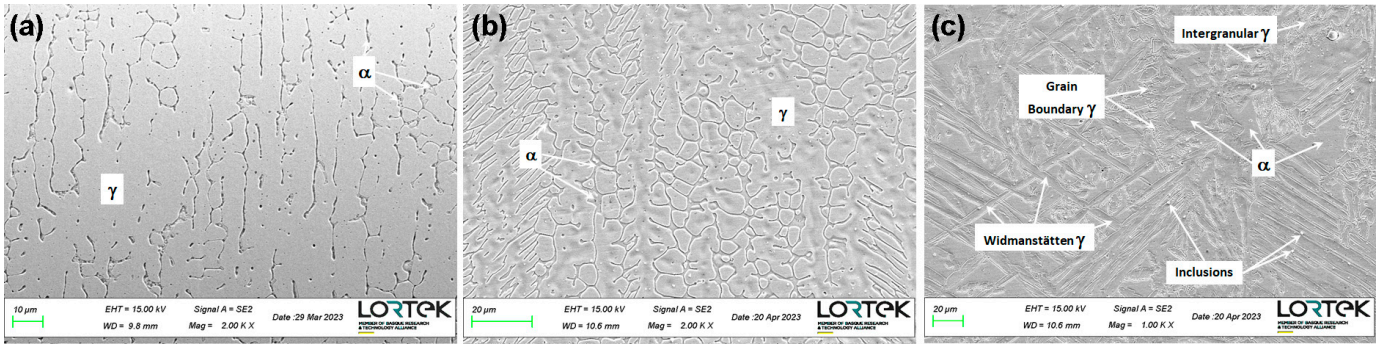

Figure 6. FESEM micrographs (SE mode, electrolytic etched cross-sections) of different SAF 2507/SS 316L mix ratios and zones in the FGM tube. (**a**) 40/60 ratio: layer 38 at a height of 18 mm, (**b**) 80/20 ratio: layer 50 at a height of 22.5 mm, and (**c**) 100/00 ratio: layer 62 at a height of 27.5 mm.

Alpha stabilizer elements such as Cr, Mo, and Fe are in higher proportion in ferrite, and elements such as Ni, Mn, Si, and N are reduced. The opposite occurs in austenite regions (see micrograph and spectrums of Figure 7 as examples of a 50/50 composition ratio).

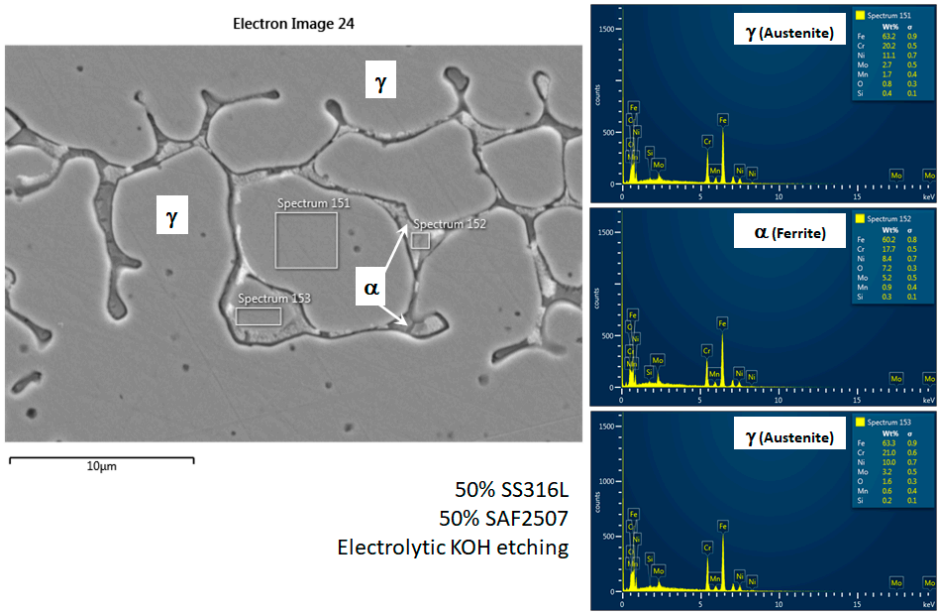

Figure 7. FESEM micrographs (SE mode, electrolytic etched cross-section) and EDS spectrums for 50% SS 316L and 50% SAF 2507 mixes (wt.%) observed in layer 33 at a height of 14.5 mm of the FGM tube.

3.4. Quantification of Austenite/Ferrite Phases

As the chemical compositional gradient increases toward that of higher super duplex content, the ferrite formation is stabilized due to the increase in the content of Cr, Mo, Fe, and Ti (alpha- or ferritizing elements) in the mixture, and with the reduction in Ni, Mn, Si, and N (gamma- or austenitizing elements). Thus, as the chemical composition of a super duplex stainless steel is approached, a balance close to ~55/45 between the two main phases observed in the microstructure (austenitic/ferritic) becomes evident. The tendency to form a greater amount of ferrite is observed in the bar graph of Figure 8 as the proportion of super duplex in the mixture increases.

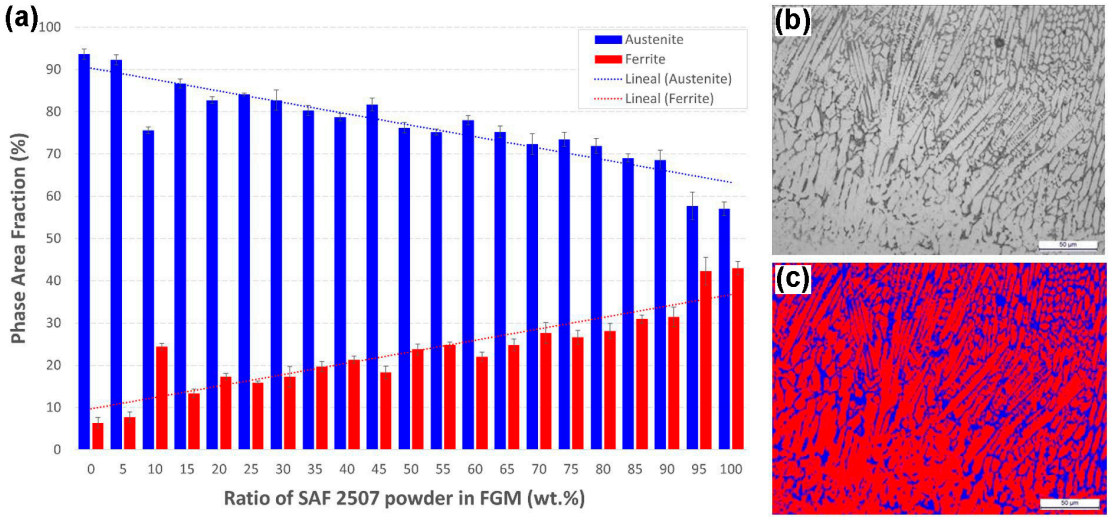

Figure 8. Evolution of the fraction of austenite and ferrite phases in the FGM SS 316L-SAF 2507 obtained by DED-LB/p. (**a**) Plot with line tendency of the calculated phase fractions, (**b**) micrograph of the 60/40 ratio, and (**c**) example of the image analysis processing for measures of phase fractions.

It was from 85% (wt.%) of super duplex content in the mixture of the FGM that a percentage of ferrite higher than 30% was obtained, which changed the dendritic morphology observed in the microstructure, and the typical "duplex" structure was formed. Better corrosion behavior was then expected from this ratio in the graded function material obtained by LMD. In the bottom layers made with 100% 316L austenitic stainless steel (first three layers), a balance of 93.61 ± 1.22% area fraction of austenite and 6.39 ± 1.22% area fraction of ferrite was obtained; the base material dilution was not considered here, while in the top layers made from 100% super duplex composition, a balance of 56.61 ± 1.86% austenite and 43.39 ± 1.62% ferrite was obtained in the resulting microstructure. This austenite/ferrite ratio measured for 100% super duplex composition layers was near to the ~55/45 reported ratios in literature for this material processed by laser [13,17,31], but lower in the ferrite area fraction than typical wrought super duplex steel (~45/55). The austenite/ferrite fraction is affected by chemical composition, solidification conditions, and cooling rates, and it is expected to have more austenite at typical deposition speeds and solidification rates in DED-LB processes in comparison with the PBF-LB process [33].

In a theoretical exercise, we calculated the theoretical austenite/ferrite phase ratio using the Schaeffler diagram and considering the chemical composition of both materials (SS 316L and SAF 2507). The measured ratio values in this work correlate well with the theoretical prediction given by the theoretical Schaeffler [34] and WRC-1992 [35] diagrams for the austenite/ferrite ratio in the welding of stainless steels. The austenitic stainless steel type 316L will have a lower resistance to pitting corrosion (PREN ~25.5) than SAF 2507 super duplex stainless steel (PREN ~42.5) according to the Schaeffler diagram [36]. Recently, other authors have concluded that the Schaffler diagram can also have a good correlation for high-energy-density welding and fast solidification processes such as laser-based directed energy deposition processes of stainless steels [26,37,38].

3.5. Micro Hardness Evolution

For the obtention of the hardness profile, the indentations were made in the central area of the tube cross-section (half of the wall thickness) and with a separation of 1.0 mm between them. Figure 9 shows the cross section of the tube wall, on which the metallographic preparation was carried out to obtain a polished surface for micro hardness measurements; the hardness profile was obtained from the build plate (SS 310), crossing the base of the tube (100% SS 316L) to the last layers of the tube (100% super duplex SAF2507 composition). An increase in hardness was evidenced by the increase in the ferrite fraction in the duplex

microstructure on the graded composition material, reaching a hardness between 217 and 230 HV for SS 316L in initial layers at the base of the tube and between 329 and 330 HV for the full super duplex composition in the last three layers of the FGM tube.

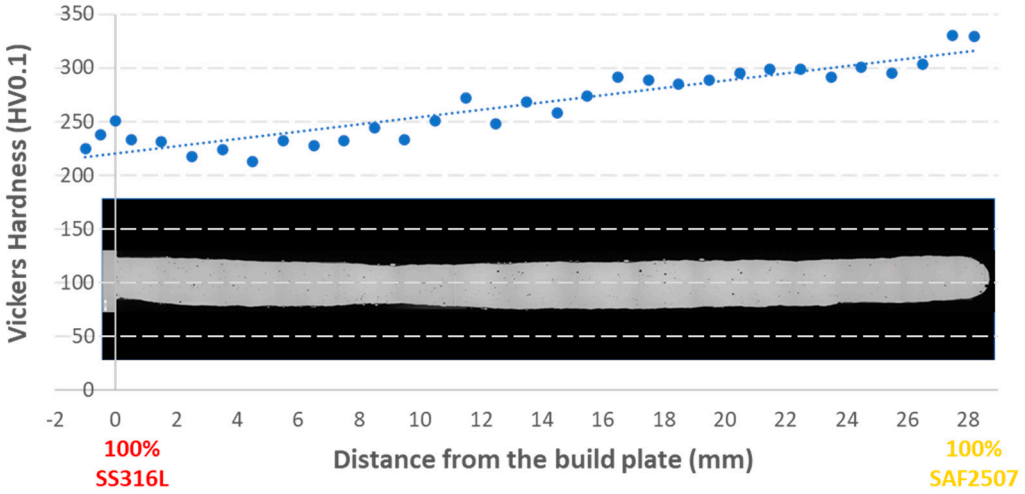

Figure 9. Macrograph of the FGM tube cross section and hardness profile.

It is well known that the nano hardness of ferrite is higher than the austenite phase in duplex and super duplex stainless steel grades [39], so the increase in the ferrite area fraction has an impact on the overall mechanical behavior of the material, which was evidenced in the microhardness measurements (HV0.1 scale) taken in this work in the cross-section of the FGM tube manufactured.

4. Conclusions

The main conclusions based on the results obtained and their analysis in this research work are as follows:

- The DED-LB/p (LMD) process is a promising manufacturing process route to obtain controlled FGMs for near-net-shape metallic components. It was demonstrated that is possible to create products with a semi-continuous functionally graded material with a gradient from austenitic to super duplex stainless-steel compositions using this technology;
- A tube with a semi-continuous functional gradient material was successfully manufactured in which the chemical composition was varied, starting from a composition of 100% austenitic stainless-steel type 316L and ending in 100% super duplex stainless-steel type SAF 2507 with a discontinuous gradient, reducing the amount of austenitic SS at 5 wt.% whilst adding 5 wt.% of the super duplex SS content in the mass flow every three layers in the manufactured single wall/bead tube;
- The evolution of ferrite formation was verified and the phase fraction measured. The increase in ferrite content is associated with the increase in alpha-iron promoter chemical elements as the proportion of super duplex steel in the powder mixture is increased. The correlation between the increase in hardness of the FGM with the increase in the ferrite phase area fraction as a hard phase in the FGM material was verified;
- It is of utmost importance to automate and control the command of the hoppers and rapid switch valves of the twin powder feeder to achieve the desired mixing ratio and powder delivery stability in the FGM obtained by DED-LB/p. The monitoring of powder flow rates using sensors and the meticulous measure of powder delays and gravimetry are essential to verify and guarantee the stability of the powder mix supply to the nozzle during the deposition process.

Author Contributions: Conceptualization, J.C.P. and M.S.S.; methodology, J.C.P.; process development and manufacturing of samples, I.T. and D.A.; Powder mixing system automation, I.T. and D.A.; Microstructure, FESEM and EDS maps analysis, R.G.; writing—original draft preparation, J.C.P.; writing—review and editing, J.C.P., R.G. and M.S.S.; project administration, J.C.P.; funding acquisition, J.C.P. and M.S.S. All authors have read and agreed to the published version of the manuscript.

Funding: This research work was supported by the Basque Government (Departamento de Desarrollo Económico e Infraestructuras, Programa ELKARTEK) through EDISON project (grant KK-2022/00070). And supported by the Ministry of Science and innovation of the Spain Government through the program "Ayudas destinadas a centros tecnológicos de excelencia CERVERA año 2019" from CDTI, in the frame of CEFAM Project (grant CER-20191005).

Data Availability Statement: The raw/processed data required to reproduce these findings cannot be shared at this time due to technical or time limitations.

Conflicts of Interest: The authors declare no conflict of interest.

References

1. Soodi, M.; Masood, S.H.; Brandt, M. Tensile strength of functionally graded and wafer layered structures produced by direct metal deposition. *Rapid Prototyp. J.* **2014**, *20*, 360–368. [CrossRef]
2. Ferreira, A.; Romio, P.; Sousa, J.; Omid, E.; Cruz, J.; Reis, A.; Vieira, M. Functionally Graded Materials (FGM) Fabricated by Direct Laser Deposition: A Review. In *Prime Archives in Material Science*; Khan, M.I., Ed.; Vide Leaf: Hyderabab, India, 2021; pp. 1–37. ISBN 978-81-953047-9-0.
3. InssTek. Actual Scale of FGM Rocket Nozzle. Available online: http://www.insstek.com/core/board.php?bo_table=news&wr_id=67 (accessed on 25 July 2023).
4. Ostolaza, M.; Arrizubieta, J.I.; Lamikiz, A.; Plaza, S.; Ortega, N. Latest Developments to Manufacture Metal Matrix Composites and Functionally Graded Materials through AM: A State-of-the-Art Review. *Materials* **2023**, *16*, 1746. [CrossRef] [PubMed]
5. Brucki, M. Environmentally Friendly Production of Tribologically Hihgly Stressed Sliding Bearings by Means of EHLA—Fraunhofer Institute for Laser Technology. Available online: https://www.ilt.fraunhofer.de/content/dam/ilt/en/documents/annual_reports/ar21/tf2/ar21-p54-environmentally-friendly-production-of-ehla.pdf (accessed on 25 July 2023).
6. Ghanavati, R.; Naffakh-Moosavy, H. Additive manufacturing of functionally graded metallic materials: A review of experimental and numerical studies. *J. Mater. Res. Technol.* **2021**, *13*, 1628–1664. [CrossRef]
7. Freeman, F.S.H.B.; Thomas, B.; Chechik, L.; Todd, I. Multi-faceted monitoring of powder flow rate variability in directed energy deposition. *Addit. Manuf. Lett.* **2022**, *2*, 100024. [CrossRef]
8. Müller, M.; Labisch, C.C.; Gerdt, L.; Bach, L.; Riede, M.; Kaspar, J.; López, E.; Brueckner, F.; Zimmermann, M.; Leyens, C. Multimaterial direct energy deposition: From three-dimensionally graded components to rapid alloy development for advanced materials. *J. Laser Appl.* **2022**, *35*, 012006. [CrossRef]
9. Yan, L.; Chen, Y.; Liou, F. Additive manufacturing of functionally graded metallic materials using laser metal deposition. *Addit. Manuf.* **2020**, *31*, 100901. [CrossRef]
10. Ansari, M.; Jabari, E.; Toyserkani, E. Opportunities and challenges in additive manufacturing of functionally graded metallic materials via powder-fed laser directed energy deposition: A review. *J. Mater. Process. Technol.* **2021**, *294*, 117117. [CrossRef]
11. Dev Singh, D.; Arjula, S.; Raji Reddy, A. Functionally Graded Materials Manufactured by Direct Energy Deposition: A review. *Mater. Today Proc.* **2021**, *47*, 2450–2456. [CrossRef]
12. Queguineur, A.; Asadi, R.; Ostolaza, M.; Valente, E.H.; Nadimpalli, V.K.; Mohanty, G.; Hascoët, J.-Y.; Ituarte, I.F. Wire arc additive manufacturing of thin and thick walls made of duplex stainless steel. *Int. J. Adv. Manuf. Technol.* **2023**, *127*, 381–400. [CrossRef]
13. Jiang, D.; Gao, X.; Zhu, Y.; Hutchinson, C.; Huang, A. In-situ duplex structure formation and high tensile strength of super duplex stainless steel produced by directed laser deposition. *Mater. Sci. Eng. A* **2022**, *833*, 142557. [CrossRef]
14. Baghdadchi, A.; Hosseini, V.A.; Valiente Bermejo, M.A.; Axelsson, B.; Harati, E.; Högström, M.; Karlsson, L. Wire Laser Metal Deposition Additive Manufacturing of Duplex Stainless Steel Components—Development of a Systematic Methodology. *Materials* **2021**, *14*, 7170. [CrossRef] [PubMed]
15. Valiente Bermejo, M.A.; Thalavai Pandian, K.; Axelsson, B.; Harati, E.; Kisielewicz, A.; Karlsson, L. Microstructure of laser metal deposited duplex stainless steel: Influence of shielding gas and heat treatment. *Weld. World* **2021**, *65*, 525–541. [CrossRef]
16. Chadha, U.; Selvaraj, S.K.; Lamsal, A.S.; Maddini, Y.; Ravinuthala, A.K.; Choudhary, B.; Mishra, A.; Padala, D.; M, S.; Lahoti, V.; et al. Directed Energy Deposition via Artificial Intelligence-Enabled Approaches. *Complexity* **2022**, *2022*, 2767371. [CrossRef]
17. Iams, A.D.; Keist, J.S.; Palmer, T.A. Formation of Austenite in Additively Manufactured and Post-Processed Duplex Stainless Steel Alloys. *Metall. Mater. Trans. A* **2020**, *51*, 982–999. [CrossRef]
18. Wen, J.-H.; Zhang, L.-J.; Ning, J.; Xue, F.; Lei, X.-W.; Zhang, J.-X.; Na, S.-J. Laser additively manufactured intensive dual-phase steels and their microstructures, properties and corrosion resistance. *Mater. Des.* **2020**, *192*, 108710. [CrossRef]

19. Altenburg, S.J.; Straße, A.; Gumenyuk, A.; Maierhofer, C. In-situ monitoring of a laser metal deposition (LMD) process: Comparison of MWIR, SWIR and high-speed NIR thermography. *Quant. Infrared Thermogr. J.* **2022**, *19*, 97–114. [CrossRef]
20. Brázda, M.; Salvetr, P.; Rzepa, S.; Melzer, D.; Vavrik, J. Effect of heat treatment on mechanical properties of duplex steel SAF 2507 manufactured by DED. *IOP Conf. Ser. Mater. Sci. Eng.* **2021**, *1178*, 12008. [CrossRef]
21. Zhang, D.; Liu, A.; Yin, B.; Wen, P. Additive manufacturing of duplex stainless steels—A critical review. *J. Manuf. Process.* **2022**, *73*, 496–517. [CrossRef]
22. Feenstra, D.R.; Banerjee, R.; Fraser, H.L.; Huang, A.; Molotnikov, A.; Birbilis, N. Critical review of the state of the art in multi-material fabrication via directed energy deposition. *Curr. Opin. Solid State Mater. Sci.* **2021**, *25*, 100924. [CrossRef]
23. Fedorov, A.; Zhitenev, A.; Strekalovskaya, D.; Kur, A. Quantitative Description of the Microstructure of Duplex Stainless Steels Using Selective Etching. *Mater. Proc.* **2021**, *3*, 4. [CrossRef]
24. Banait, S.M.; Paul, C.P.; Jinoop, A.N.; Kumar, H.; Pawade, R.S.; Bindra, K.S. Experimental investigation on laser directed energy deposition of functionally graded layers of Ni-Cr-B-Si and SS316L. *Opt. Laser Technol.* **2020**, *121*, 105787. [CrossRef]
25. Zhang, K.; Wang, S.; Liu, W.; Shang, X. Characterization of stainless steel parts by Laser Metal Deposition Shaping. *Mater. Des.* **2014**, *55*, 104–119. [CrossRef]
26. Smith, T.R.; Sugar, J.D.; San Marchi, C.; Schoenung, J.M. Microstructural development in DED stainless steels: Applying welding models to elucidate the impact of processing and alloy composition. *J. Mater. Sci.* **2021**, *56*, 762–780. [CrossRef]
27. Pandey, P.K.; Singh, M.; Rathi, R.; Verma, J. Analysis and optimization of welding techniques for austenitic stainless steel using grey relational analysis. *Int. J. Interact. Des. Manuf.* 2023; *in press*. [CrossRef]
28. Yamashita, S.; Yamauchi, R.; Saida, K. Influence mechanism of solidification mode on solidification cracking susceptibility of stainless steel. *Weld. Int.* **2022**, *36*, 693–704. [CrossRef]
29. David, S.A. *Ferrite Morphology and Variations in Ferrite Content in Austenitic Stainless Steel Welds*; Oak Ridge National Lab.: Oak Ridge, TN, USA, 1981.
30. Elmer, J.W.; Allen, S.M.; Eagar, T.W. Microstructural development during solidification of stainless steel alloys. *Metall. Trans. A* **1989**, *20*, 2117–2131. [CrossRef]
31. Iams, A.D.; Keist, J.S.; Giannuzzi, L.A.; Palmer, T.A. The Evolution of Oxygen-Based Inclusions in an Additively Manufactured Super-Duplex Stainless Steel. *Metall. Mater. Trans. A* **2021**, *52*, 3401–3412. [CrossRef]
32. Leone, G.L.; Kerr, H.W. The ferrite to austenite transformation in stainless steels. *Weld. J.* **1982**, *61*, 13S–21S.
33. Saeidi, K.; Kevetkova, L.; Lofaj, F.; Shen, Z. Novel ferritic stainless steel formed by laser melting from duplex stainless steel powder with advanced mechanical properties and high ductility. *Mater. Sci. Eng. A* **2016**, *665*, 59–65. [CrossRef]
34. Schaeffler, A.L. Constitution Diagram for Stainless Steel Weld Metal. *Met. Prog.* **1949**, *56*, 680.
35. Kotecki, D.J.; Siewert, T.A. WRC-1992 constitution diagram for stainless steel weld metals: A modification of the WRC-1988 diagram. *Weld. J.* **1992**, *71*, 171–178.
36. Guiraldenq, Pierre; Hardouin Duparc, Olivier The genesis of the Schaeffler diagram in the history of stainless steel. *Met. Res. Technol.* **2017**, *114*, 613. [CrossRef]
37. David, S.A.; Vitek, J.M.; Reed, R.W.; Hebble, T.L. *Effect of Rapid Solidification on Stainless Steel Weld Metal Microstructures and Its Implications on the Schaeffler Diagram*; Report No. ORNL/TM-10487; Oak Ridge National Lab.: Oak Ridge, TN, USA, 1987.
38. Nedjad, S.H.; Yildiz, M.; Saboori, A. Solidification behaviour of austenitic stainless steels during welding and directed energy deposition. *Sci. Technol. Weld. Join.* **2023**, *28*, 1–17. [CrossRef]
39. Argandoña, G.; Palacio, J.F.; Berlanga, C.; Biezma, M.V.; Rivero, P.J.; Peña, J.; Rodriguez, R. Effect of the Temperature in the Mechanical Properties of Austenite, Ferrite and Sigma Phases of Duplex Stainless Steels Using Hardness, Microhardness and Nanoindentation Techniques. *Metals* **2017**, *7*, 219. [CrossRef]